JOURNAL OF MATERIALS PROCESSING TECHNOLOGY 209 (2009) 3050–3059

journal homepage: www.elsevier.com/locate/jmatprotec

Extrusion of 7075 aluminium alloy through double-pocket dies to manufacture a complex profile

Gang Fang[1], *Jie Zhou*[*], *Jurek Duszczyk*

Department of Materials Science and Engineering, Delft University of Technology, Mekelweg 2, 2628 CD Delft, The Netherlands

ARTICLE INFO

Article history:
Received 7 February 2008
Received in revised form 5 June 2008
Accepted 5 July 2008

Keywords:
Aluminium
Extrusion
Die
FEM simulation

ABSTRACT

Low-temperature incipient melting and high deformation resistance of aluminium alloy AA7075 place extraordinary demands on extrusion die design and process optimization, especially when the shape of the extrudate is complex. The present case study was aimed at combining the considerations on die design and process optimization for the alloy to manufacture a complex solid profile with large differences in wall thickness, by means of 3D FEM simulation and experimentation instead of the traditional trial and error approach. The effects of die bearing length and extrusion speed on extrudate temperature and extrusion pressure were predicted. The results of the simulations clearly indicate that for AA7075 extrusion speed has a strong effect on extrudate temperature and the latter largely determines the surface quality of the extruded profile. A longer die bearing allows more heat to dissipate from the extrudate to the colder die and leads to a greater extrudate dimensional accuracy. The effects of die bearing length and extrusion speed on extrusion pressure are however insignificant. Thus, the extrusion throughput is mainly limited by the extrudate temperature rather than extrusion pressure. The case study demonstrates that 3D FEM simulation is a viable predictive tool for both die design and process optimization and the approach is applicable to the extrusion of other alloys for any other extrudate shapes.

1. Introduction

AA7075 is a high-strength aluminium alloy extensively used for highly stressed structural components in the aerospace, aircraft and defence industries. It is generally acknowledged that the alloy is very difficult to extrude, especially when the cross-section shape of the extrudate is complex. For this alloy, the optimization of the extrusion process in terms of reaching a maximum extrusion speed without jeopardizing extrudate surface and microstructural quality is far more complex than in the case of extruding 6xxx series aluminium alloys (Dixon, 2000). Extrusion speed applicable to AA7075 (1–2 m/min) is only a small fraction of that for a medium-strength 6xxx series alloy such as AA6061 (5–25 m/min) (Dixon, 2000). The low extrudability of AA7075 is related to its chemical composition with zinc, magnesium and copper as the main alloying elements (Zakharov, 2005). On the one hand, the extrusion speed applicable is limited by the low incipient melting temperature (477 °C) of the alloy, as a result of incomplete dissolution of low melting point phases (*i.e.* AlMgZnCu eutectic phases) during the homogenization of billets, following direct-chill casting. The chance of resulting in speed cracking or even hot shortness at 480–485 °C, especially in critical regions such as the tips of an extruded profile, is great. On the other hand, the extrusion speed applicable to AA7075 is restricted by high pressure required for breakthrough, especially when reduction ratio is

* *Corresponding author*. Tel.: +31 15 278 5357; fax: +31 15 278 6730.
E-mail address: j.zhou@tudelft.nl (J. Zhou).
[1] Present address: Department of Mechanical Engineering, Tsinghua University, Beijing 100084, China.
0924-0136/$ – see front matter © 2008 Elsevier B.V. All rights reserved.
doi:10.1016/j.jmatprotec.2008.07.009

high in the case of manufacturing a complex profile with thin walls. Compared with other aluminium alloys, AA7075 has higher flow stresses that are sensitive to strain rate and temperature (Lee et al., 2000). Although extrusion in the indirect mode can effectively reduce the pressure required for extrusion, due to the elimination of the friction at the container wall (Sheppard et al., 1982), the process requires scalped billets and, moreover, has limited freedom in permitting a wide range of extrudate cross-section shapes. Therefore, across the aluminium extrusion industry, extrusion in the direct mode is predominantly applied to the AA7075 alloy for solid extrudates. Both the great risk of resulting in defects and the high demand for extrusion pressure leave the press operator with no choice but a very low extrusion speed at the expense of extrusion throughput. The choice of "safe" process parameters is based on the experience of the press operator who has no predictive tools, except trial and error.

An additional limit to the extrusion speed applicable is imposed by an undesirable coarse grain structure at the periphery of the extruded product, which is mainly caused by temperatures raised locally, resulting from friction with the die, in combination with high strain-rate deformation at the die entrance. A peripheral coarse grain structure leads to lowered mechanical properties and stress-corrosion cracking resistance of the extruded product. When this occurs, the extruded product may have to be scraped. Obviously, the only preventive measure is to predict the local temperatures of the extrudate on the cross-section and along the length for a given set of process parameters, which has not been possible across the aluminium extrusion industry yet.

The design of extrusion die plays a crucial role in determining the scope of the interplay between extrusion speed and billet temperature to optimize the extrusion process and to avoid the surface and microstructure defects, in addition to dimensional accuracy. This is because extrusion pressure and extrudate temperature are both closely related to metal flow at the die bearing and in turn to die design. In the open literature on the extrusion of high-strength aluminium alloys, few publications address the issue of extrusion die design in relation to process optimization for the AA7075 alloy, except the common sense that die support, especially the support for die tongues, must be strengthened in order to resist high stresses acting on the die face (Dixon, 2000). The missing link between extrusion die design and extrusion process optimization is mainly because these are two business activities taking place often not under the same roof. Die design is, in general, considered the proprietary knowledge of the die designer. Extrusion process optimization is the task of the extrusion process engineer. These two are often not communicative, mainly because they have no common predictive tools.

The current understanding of metal flow through extrusion die is mostly based on the earlier research on plane or axi-symmetric extrusion of sheet or rod, using analytical and semi-analytical methods such as the slip line, integral profile, upper bound and ideal work methods (Johnson and Kudo, 1962). Undoubtedly, the research contributes to a fundamental understanding of the extrusion process, especially the metal flow patterns in the case of extrusion to produce sheets, rods or very simple profiles. These methods have, however, a limited scope to incorporate thermal effects into the process, thus being of limited practical use to guide the die designer and extrusion process engineer in optimizing die design and the process to extrude the AA7075 alloy into complex profiles.

The recent rapid developments in the process simulation technology based on the finite element method (FEM) have made detailed analysis of metal flow during extrusion possible. For example, physical modelling was combined with 2D FEM simulation of cold extrusion involving plane strain and axi-symmetric geometries (Arentoft et al., 2000). Gouveia et al. (2001) succeeded in 3D FEM simulation of extrusion to produce a square profile and compared their simulation results with those from physical modelling. Li et al. (2003a) studied the influence of pocket die design on metal flow in aluminium extrusion by means of 2D FEM simulation under the isothermal condition. Lee et al. (2002) applied 3D FEM simulation of extrusion through flat dies with thermal effects incorporated. Li et al. (2003b) used 3D FEM simulation to predict extrudate temperatures at various extrusion speeds for a given die bearing setting. A multi-hole pocket die with four L-shaped openings and different pocket shapes has recently been used to evaluate the capabilities of different FEM software packages. The results are quite encouraging, although further research with improved physical and numerical parameters is needed to achieve a better agreement between FEM predictions and experimental data (Shikorra et al., 2007). The ALE (Arbitrary Lagrangian Eulerian) adaptive meshing method has shown its capabilities of predicting metal flow and the final shape of the product effectively and efficiently, although it is still under development (Kayser et al., 2008). Unfortunately, there have been no studies on metal flow through extrusion dies of industrial significance in relation to extrusion process optimization. In this connection, FEM simulation has generally been considered a potential tool primarily for the die designer. The genuine interest in FEM simulation of extrusion for process optimization is yet to be developed.

The present case study was intended to demonstrate for the first time that, in the case of extruding the AA7075 alloy into a complex profile with varied wall thicknesses, the design of extrusion die and the choice of process parameters could be integrated by means of 3D computer simulation to achieve optimum product quality and maximum throughput. Three double-pocket dies with different bearing lengths were designed and extrusion speed was varied. Extrudate temperature, extrusion pressure requirement and surface quality were predicted and experimentally validated. The knowledge gained is expected to be transferred to similar forming processes for this high-strength aluminium alloy and the novel approach to be extended to the extrusion of other alloys for any other extrudate shapes.

2. Design of double-pocket dies with different bearing settings

Fig. 1 shows the cross-section shape and dimensions of the profile used in the present case study. It is a typical industrial profile with tips and thin walls, thus presenting quite a challenge to the die designer and extrusion process engineer, because it exerts great pressures on the die tongues, undergoes large, inhomogeneous deformation and restricts

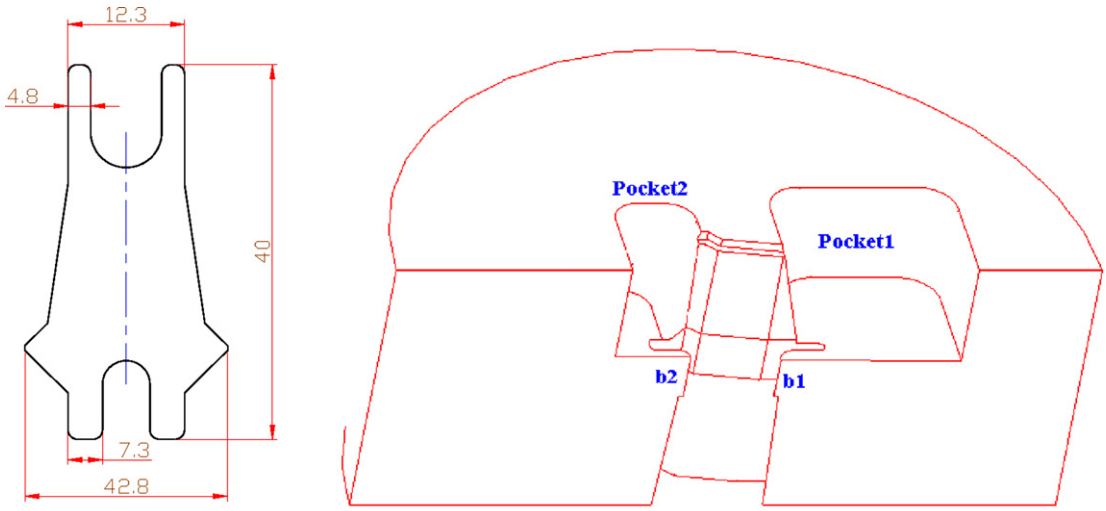

Fig. 1 – Cross-section shape and dimensions of the extrudate and the basic design of the double-pocket die (half model) (b1—die bearing 1 behind Pocket 1 and b2—die bearing 2 behind Pocket 2).

Table 1 – Die bearing lengths behind Pocket 1 and Pocket 2

	Bearing b1 [mm]	Bearing b2 [mm]
Die No. 1	2.5	3.5
Die No. 2	5.0	6.0
Die No. 3	10.0	11.0

extrusion speed to be applied. To assist in balancing metal flow through the die with very large differences in opening size (from 4.8 to 42.8 mm), double pockets (Pocket 1 and Pocket 2 in Fig. 1) were assigned to the upper part and the lower part of the die orifice. These two pockets were used in combination with varied die bearing lengths to regulate metal flow through the die. Pocket 1 with a greater depth in combination with a shorter die bearing length was intended to facilitate the metal flow at the thinner tip (4.8 mm). Pocket 2, being shallower, in combination with a relatively long die bearing length was intended to facilitate the metal flow at the thicker tip (7.3 mm), but to a less extent. In the middle part of the profile, a long die bearing choked at an angle 3° was used to detain the metal flow, as a choked deep bearing is known for being able to slow down the metal flow and help to minimise the depth of the peripheral coarse grain structure (Dixon, 2000). The inner walls of the pockets near the die centre had a 15° choked angle, which was intended to balance the metal flow there in connection with the central part of the profile. To evaluate the effect of die bearing length on metal flow, extrudate temperature and extrusion pressure requirement, three double-pocket dies with bearing lengths as given in Table 1 but unvaried pocket volumes were designed.

3. FEM simulation procedures and experimental conditions

DEFORM 3D, an FEM-based commercial software package, was used to simulate the extrusion of the 7075 aluminium alloy through the three double-pocket dies with different bearing length settings (Table 1). The software adopts implicit FEM to calculate the rigid-visco-plastic deformation behaviour of the workpiece with thermal effects incorporated, which is especially suitable for the simulation of hot extrusion as in the present case study. The flow stress data of the AA70575 alloy in the ASM Hot Working Guide (Prassad and Sasidhara, 1997) were used as the input material data for the FEM simulations. Its physical properties are given in Table 2. The die and other extrusion tooling (stem and container) were assumed to be rigid and made of the H13 tool steel with their physical properties as given in Table 2. Their thermal interactions with the workpiece in the form of conduction were incorporated in the FEM simulations, and so were the thermal transfer within the workpiece, die and other extrusion tooling. The boundary conditions for the heat transfer between the objects (workpiece, die and other extrusion tooling) and the ambient atmosphere (air) took convection and radiation into account. The heat transfer coefficients and emissivity specified are given in Table 2.

In hot extrusion of aluminium alloys, friction is a highly complex thermo-tribological phenomenon. It has been acknowledged as the most uncertain parameter in the FEM

Table 2 – Physical properties of the workpiece and extrusion tooling and heat transfer coefficients

Physical properties	AA7075	H13 tool steel
Heat capacity [N/(mm² °C)]	2.39	5.6
Thermal conductivity [W/(m °C)]	130	28.4
Heat transfer coefficient between tooling and workpiece [N/(°C s mm²)]	11	11
Heat transfer coefficient between tooling/workpiece and air [N/(°C s mm²)]	0.02	0.02
Emissivity	0.1	0.7

Table 3 – Process parameters and billet dimensions used in FEM simulation and experiments

Initial temperature (°C)	
Die	450
Stem	450
Container	450
Billet	470
Ram speed [mm/s]	0.4, 0.6
Extrusion speed [m/min]	0.51, 0.76
Billet diameter [mm]	110
Billet length [mm]	220
Extrusion ratio	21.23

simulation of aluminium extrusion. In the present research, the shear friction mode was assumed to represent the friction between the workpiece and die and between the workpiece and container/stem:

$$f_s = mk \quad (1)$$

where f_s is the frictional stress, k the shear yield stress of the deforming workpiece and m the friction factor. A friction factor of 0.40 was assumed at the interface between the workpiece and die, representing the sliding contact, and 0.85 between the workpiece and container/stem, representing the nearly sticking contact, as commonly observed in aluminium extrusion practice and confirmed by Flitta and Sheppard (2003).

Geometric models of the billet, die and other extrusion tooling were built in CAD software. According to the geometrical and boundary conditions of extrusion to manufacture the solid profile as shown in Fig. 1, one half of the geometric models were constructed. Four-node tetrahedron elements were generated for thermo-mechanical calculations. Because of the large dimensional differences between the billet (Table 3) and the profile with thin-wall tips (Fig. 1), adaptive meshing of the workpiece was necessary. To limit the element number and at the same time to ensure calculation accuracy, the regions of the workpiece with large deformation had finer meshes, while other regions had coarser meshes. Die meshes were only used to calculate thermal effects. The meshes near the die opening were finer than those in the other regions of the die. Remeshing was controlled by the distortion degree of the workpiece meshes and the intersections between the workpiece and die. Fig. 2 illustrates the meshed billet, die and other extrusion tooling.

The extrusion process parameters and the dimensions of the billet used in the FEM simulations are listed in Table 3, which were the same as those used in experimental verification. A quite high billet temperature of 470 °C was deliberately chosen in order to approach the critical condition where hot shortness was expected to occur (480–485 °C) to the AA7075 alloy homogenized under the industrial conditions. The surface appearance of the extrudate along its length would then provide information supplementary to temperature measurements by means of a multi-wavelength pyrometer at the press exit. In addition, a high billet temperature would allow local flow inhomogeneity to manifest itself better, thereby facilitating the comparison between the results from the FEM simulations and extrusion experiments.

FEM simulations were performed with an AMD quad processor workstation. The number of the elements of the workpiece approached 200,000, when the extrudate emerged from the die. For the designer, the shape of the front end of an extruded profile indicates the quality of the die design. For the extrusion process engineer, the breakthrough pressure decides if a given set of extrusion parameters is applicable in practice. Thus, the extrusion in the transient state is of main interest, as compared with that in the steady state. It is certain that the extrudate temperature evolves further in the steady state, as demonstrated by Zhou et al. (2003) in the case of extrusion to produce a simple solid profile on the laboratory scale. With the state-of-the-art computing hardware, the simulation of the extrusion process on the industrial scale to manufacture a complex profile requires frequent remeshing, takes a very long time and generate a huge amount of data. As the main objective of the present research was to evaluate the effects of die bearing length and ram speed on metal flow, extrudate temperature and peak extrusion pressure, in this study, the FEM simulations were limited to the transient state of the extrusion process till the extrusion pressure peak was over.

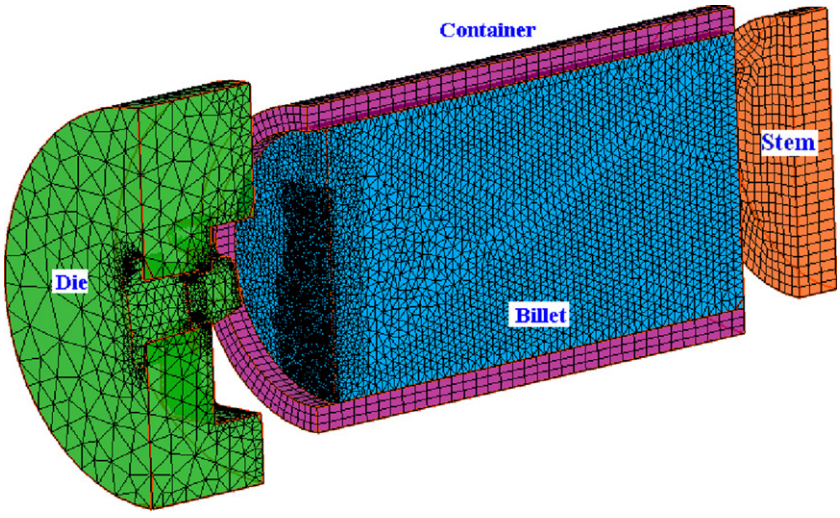

Fig. 2 – FEM meshes of the billet, die and other extrusion tooling.

Fig. 3 – Example of a double-pocket die used in extrusion experiments.

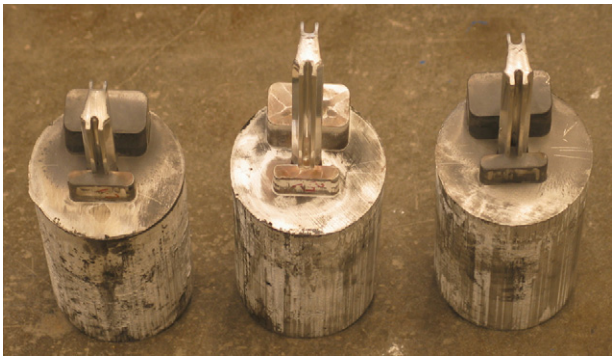

Fig. 4 – Billet material filled in the pockets of the dies with three different bearing lengths.

Extrusion experiments were performed under the conditions identical to those used in the FEM simulations (Table 3). An example of the double-pocket die designed and manufactured is shown in Fig. 3. Fig. 4 shows the billet material filled in the three dies with different bearing lengths but the same pocket volumes. A 600 tonne extrusion press equipped with a data acquisition system to register extrusion force, die temperature and extrudate temperature was used for the experiments. A 3T AE3000 pyrometer was placed at the press exit and the measuring spot was about 1200 mm away from the die bearing outlet, as constrained by the press construction and die assembly —a situation typical of industrial extrusion presses. This location excluded the radiations from other heat sources such as heated die and its associated tooling, ensuring the accuracy and repeatability of the temperature measurement of the extrudate within ±1%. The temperature measured was an average value within the spot with a diameter of 20 mm, as the lens of the pyrometer was placed about 1 m above the profile running out of the press. As extrusion experiments were performed in the billet-on-billet semi-continuous fashion after a thermal balance of the press was reached, the temperature profile along the length of the extrudate could be captured.

In addition to extrusion in the billet-on-billet fashion to manufacture the solid profile of the whole length, some extrusion runs were stopped at a ram displacement of 5 mm in order to capture the extrudate front end just emerging from the die.

4. Results and discussion

4.1. *Extrudate front end*

Flow inhomogeneity is clearly manifested in the shape of the extrudate front end. Fig. 5 shows a comparison between an experimentally obtained extrudate front end and an FEM simulated one, when extrusion through Die No. 2 was performed at a ram speed of 0.6 mm/s corresponding to an extrusion speed (or exit speed) of 0.76 m/min (Table 3). From both simulation and experimental results, it is clear that the metal in the middle of the profile still flowed faster than that at the profile tips, although the double pockets and the shorter bearings were assigned. The metal at the thinner tips flowed even more slowly than that at the thicker tips. The non-uniform metal flow resulted in the slight bending of the extrudate, as shown in Fig. 5, and the curvatures of the profiles from the simulation and experiment in terms of the radius are quite similar to each other (*i.e.* a difference of 0.6%).

The non-uniform metal flow led to inhomogeneous strains inside the extrudate. Fig. 6 shows the distribution of the effective strains on the cross-section of the extrudate. It is clear that severer deformation occurs at the thinner tips of the profile than in the other regions.

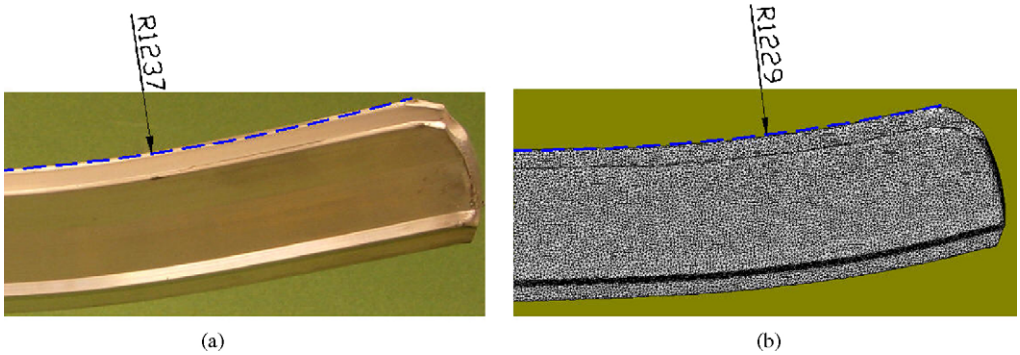

Fig. 5 – (a) Experimental and (b) simulated extrudate front ends through Die No. 2 with a difference of 0.6% in the radius of the curvature.

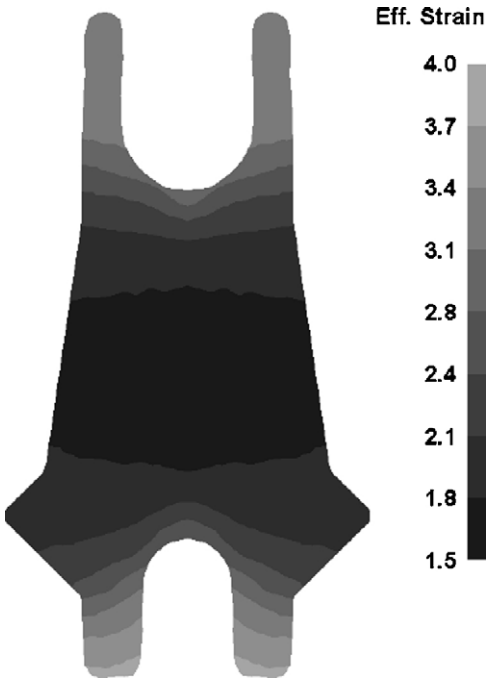

Fig. 6 – Effective strain distribution on the cross-section of the extrudate.

The velocity distributions of the extrudate on the longitudinal and cross-sections are shown in Fig. 7a and b, respectively. The velocity differences between the tips and the middle of the extrudate led to a 'snake head' shape of the front end. The velocity distributions of the extrudates through the other two pocket dies are quite similar to those shown in Fig. 7.

Fig. 8 presents a comparison between the extrudate front ends emerging from the three pocket dies with different bearing lengths in terms of extrudate dimensional stability. It is of interest to see that Δd in Fig. 8 denoting the dimensional change of the extrudate decreases with increasing bearing length. It means that a longer die bearing contributes to a greater dimensional accuracy. The dimensional change is because the extrudate shrinks when it exits from the die. It is now clear that the extent of this shrinkage becomes less with increasing die bearing length.

4.2. *Temperature evolution*

The temperature distributions of the workpiece along with ram displacement are shown in Fig. 9. In this particular FEM simulation of extrusion through Die No. 2 with bearing lengths of 5 and 6 mm after the two pockets (Table 1), the ram speed used was 0.6 mm/s. It can be seen that, while the metal was filling the pockets (Fig. 9a), the temperatures of the billet were lower than the initial billet temperature (470 °C). When the metal arrived at the middle of the pockets, the local temperatures were brought back to the initial billet temperature. This thermal phenomenon is because at the beginning of extrusion the hotter billet (470 °C) contacted the colder extrusion die (450 °C) and heat dissipation took place. At the stage of filling the conical pockets, deformation was very small and, as a result, local temperature rise (in the range of 2.87–3.41 °C) caused by plastic deformation was marginal. When the metal flowed into the die bearing, the workpiece temperature increased rapidly from 470 to 480 °C (Fig. 9b) as a result of large deformation. Along with ram advancing further, the temperature of the metal near the die bearing continued to rise (Fig. 9c) and reached a value 494 °C at a ram displacement of 12.1 mm.

The maximum temperature of the workpiece is critical to the surface quality of the extrudate and also to its microstructure. The evolution of the maximum temperature of the workpiece in the transient state of extrusion is shown in Fig. 10 where the three different die designs and two ram speeds are compared. It shows the initial decrease of the maximum temperature during the filling of the pockets, as discussed earlier. Of more interest are the rapid temperature rise, as a combined result of large deformation and friction, and the magnitude of

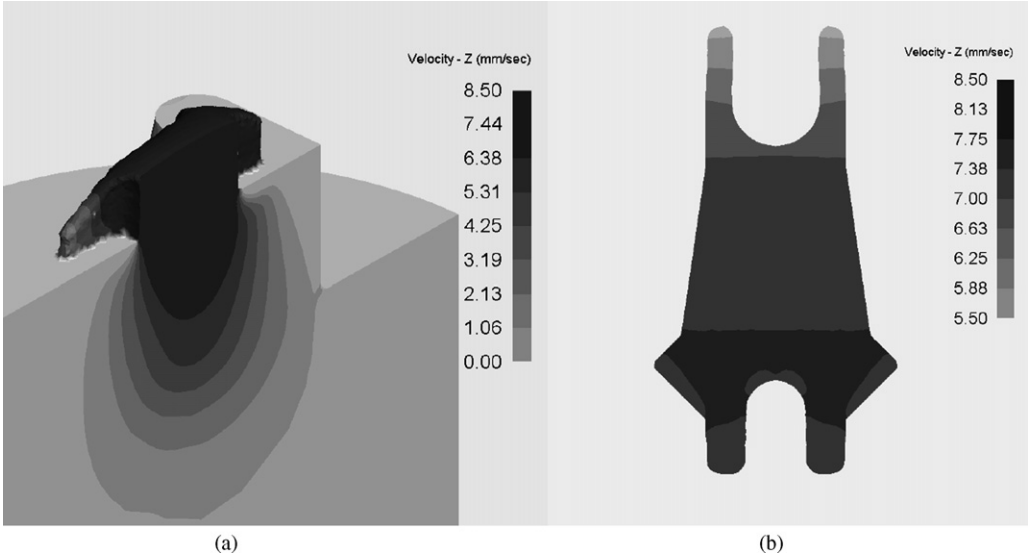

Fig. 7 – Velocity distributions of the workpiece passing through Die No. 2 at an extrusion speed of 0.51 m/min: (a) longitudinal section and (b) cross-section.

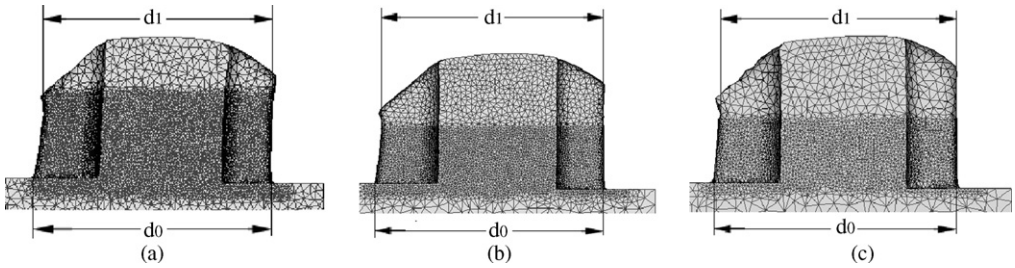

Fig. 8 – Dimensional change of the extrudate after exiting from the three double-pocket dies with different bearing lengths at an extrusion speed of 0.76 m/min: (a) Through Die No. 1, $d_0 = 40.08$; $d_1 = 38.42$; $\Delta d = 1.66$, (b) through Die No. 2, $d_0 = 40.06$; $d_1 = 38.56$; $\Delta d = 1.50$ and (c) through Die No. 3, $d_0 = 39.70$; $d_1 = 38.75$; $\Delta d = 0.95$.

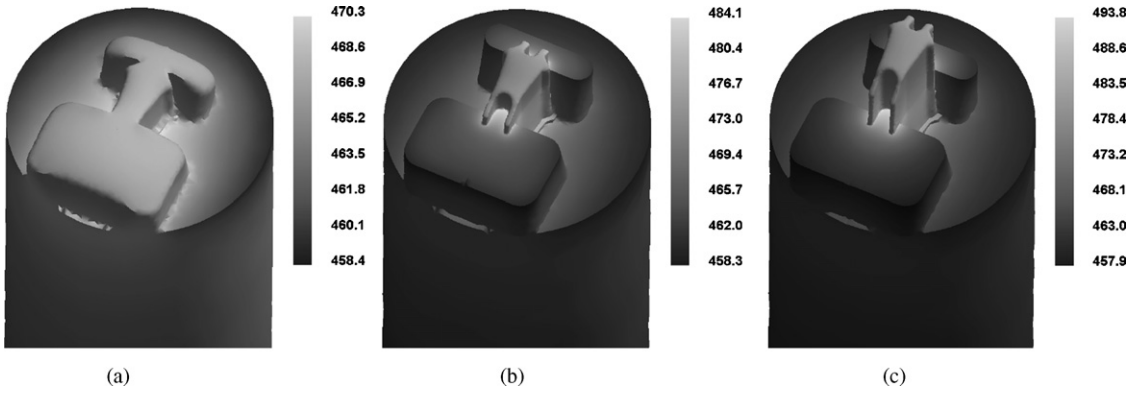

Fig. 9 – Temperature distributions of the workpiece during extrusion through Die No. 2 with bearing lengths of 5 and 6 mm and at a ram speed of 0.6 mm/s (s—ram displacement): (a) $s = 9.45$ mm, (b) $s = 11.10$ mm and (c) $s = 12.10$ mm.

this temperature rise in relation to die bearing length and ram speed. It is clear that with the same die design, ram speed has a profound effect on the maximum extrudate temperature. An increase in ram speed from 0.4 (curves A1, A2 and A3) to 0.6 mm/s (curves B1, B2 and B3) leads to considerable maximum temperature increases. It is important to note that when the maximum workpiece temperature is close to the incipient melting point of the AA7075 aluminium alloy, such a temperature rise becomes crucial, deciding if the extruded profile will be scrap or a saleable product.

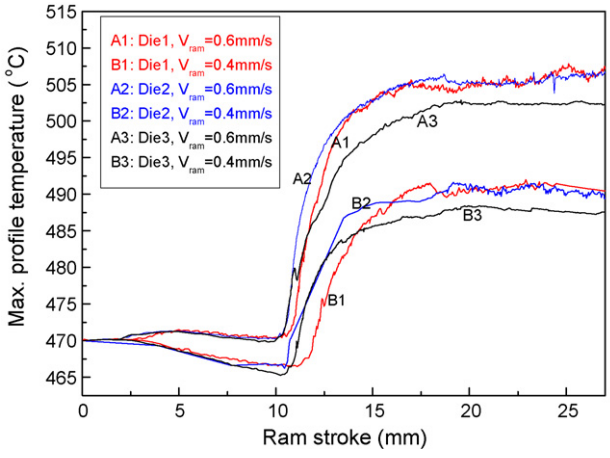

Fig. 10 – Evolutions of the maximum temperatures of the workpiece through the three dies and at extrusion speeds of 0.51 and 0.76 m/min (simulation results).

The evolution of the maximum temperature is due to the friction with the die, the deformation inside the workpiece and the thermal interactions with the die. Fig. 10 shows that at the same ram speed, die design clearly has an effect on the maximum workpiece temperature. In the case of Die No. 3, due to its longer die bearings (10 and 11 mm behind Pocket 1 and Pocket 2, respectively, see Table 3), the deforming material had the lowest maximum temperature. It suggests that the heat dissipation from the workpiece (initially at 470 °C) to the die (initially at 450 °C) due to a larger contact area at the die bearing was more significant than the additional friction-generated heat. The maximum temperature occurs at the die bearing inlet, as will be shown later, indicating that the heat converted from deformation is far more pronounced that the heat generated from the friction at the die bearing.

A detailed analysis of the die temperature evolution at the sampling points: bearing inlet A and bearing outlet B, is given in Fig. 11. For both Die No. 1 and No. 3, the temperature increases at the bearing outlet B are of smaller amplitude than at the bearing inlet A. It was thought that the metal would be constrained while flowing along the die bearing. Severe deformation and friction at the die bearing would lead to further temperature rises at the bearing outlet. However, because the bearing outlet B is exposed to the ambient temperature, it has

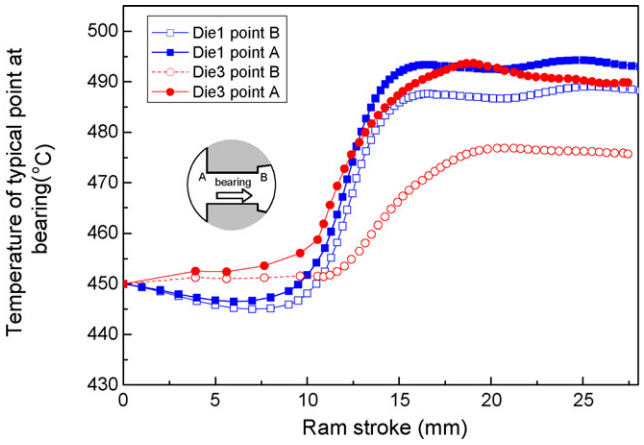

Fig. 11 – Temperature evolutions at the die bearing inlet and outlet during extrusion at a ram speed of 0.6 mm/s (simulation results).

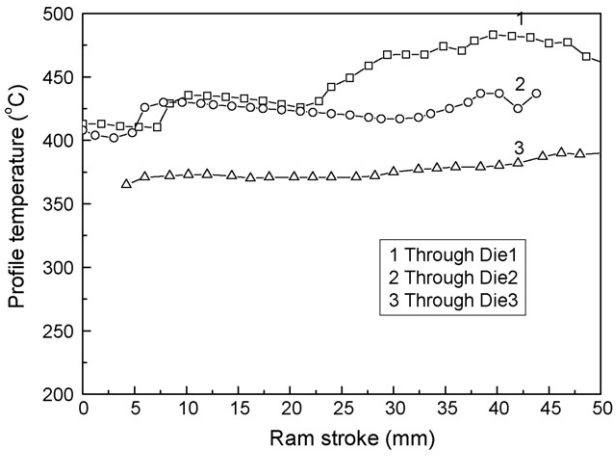

Fig. 12 – Evolutions of the extrudate temperatures measured at the press exit (ram speed 0.6 mm/s, experimental results).

consistently lower temperatures than the bearing inlet A. As the extrusion process proceeds, the temperatures at both the bearing inlet and outlet approach a steady state, right after the metal exits from the die. Fig. 11 also shows that the temperature rises at both of these two sampling points in Die No. 1 are more pronounced than those in Die No. 3. This is because the former has shorter bearing lengths. However, up to a ram displacement of 9 mm, the temperatures of the bearing of Die No. 3 are slightly higher than those of Die. No. 1. This is because over this ram displacement, the billet fills the pockets before reaching the die bearing and Die No. 3 has a longer bearing and shallower pockets, thus losing less heat to the atmosphere. As soon as the extrusion starts (after a ram displacement of 9 mm), the variation of die temperature with bearing length becomes the same as that of extrudate temperature; a longer die bearing leads to a lower die temperature and also a lower extrudate temperature.

Fig. 12 shows the temperatures of the extrudates experimentally measured during extrusion through the three extrusion dies designed. It is clear that the temperatures of the extrudate through Die No. 3 are at the lowest level, which is in agreement with the FEM predictions. The temperatures of the profile through Die No. 1 are almost the same as those through Die No. 2, being consistent with the FEM simulation results. However, as ram advances further, these two temperature curves tend to diverge. This is likely because the shorter bearing lengths in Die No. 1 allow less heat to dissipate to the colder die, as the temperature difference between the die and extrusion and thus the driving force for heat dissipation vanish, leading to extrudate temperature increases after a thermal balance between the extrudate and die is reached. In comparing Fig. 12 with Fig. 10, it is important to note that Fig. 10 gives the maximum temperatures of the workpiece, while Fig. 12 gives the average temperatures of the extrudate at the press exit at 1200 mm away from the die bearing outlet. Still, Fig. 12 shows the effect of die design on the extrudate temperature, being consistent with the predictions from the FEM simulations.

As mentioned earlier, surface defects are expected to appear when the extrudate temperature exceeds a critical value. Fig. 13 shows that the surface of the extrudate deteriorated as the process at a ram speed of 0.6 mm/s proceeded. The beginning part of the extrudate was good (Fig. 13a), then mini-cracks appeared at the tips of the profile (Fig. 13b) and finally hot shortness occurred also at the tips of the profile (Fig. 13c), regardless of the die design. At the lower ram speed (0.4 mm/s), however, these defects did not appear. This experimental observation is consistent with the predictions of the temperatures of the extrudate at the die exit (Fig. 9). Mini-cracks occur when the tensile stresses at the extrudate tips exceed a critical value of the billet material (fracture strength). Although the exact fracture strengths of the alloy at high temperatures are unknown, the FEM simulations revealed marked differences in the maximum principle stress; an increase in

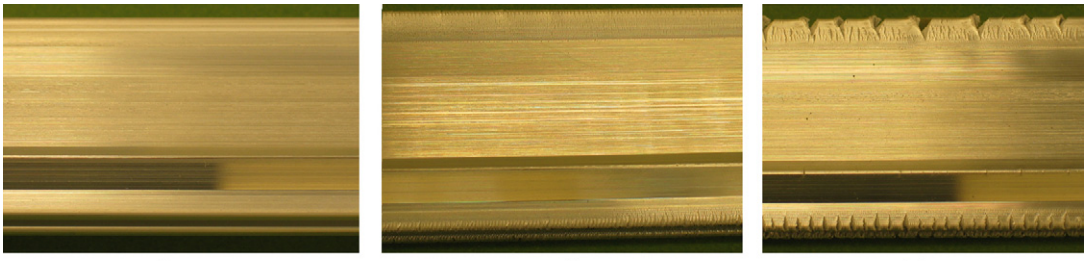

Fig. 13 – Extrudate surface quality determined mainly by the temperatures at the extrudate tips: (a) perfect surface, (b) surface with mini-cracks and (c) surface with hot shortness.

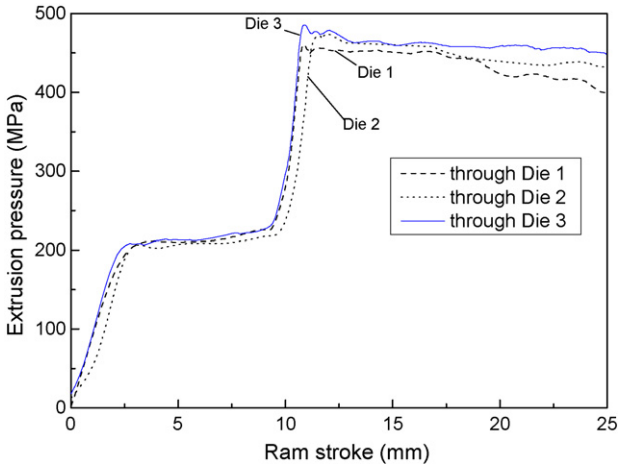

Fig. 14 – Pressure evolutions during extrusion through the three double-pocket dies and at a ram speed of 0.6 mm/s (simulation results).

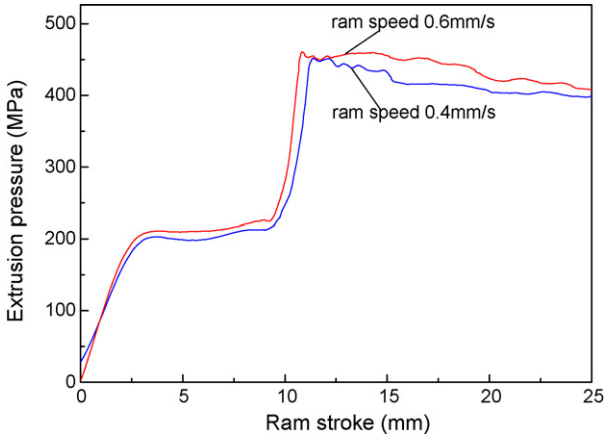

Fig. 15 – Pressure evolutions during extrusion through Die No. 2 and at ram speeds of 0.4 and 0.6 mm/s (simulation results).

ram speed from 0.4 to 0.6 mm/s, for example, would lead to an increase in the maximum principle stress by 76% in the case of extrusion through Die No. 2. A shorter bearing length tended to increase the maximum principle stress; a reduction of bearing length from 10 to 2.5 mm increased the maximum principle stress by 65%. However, temperature must have been a more important factor deciding the surface quality of the extrudate. Large deformation at the tips of the profile, as shown in Fig. 6, caused local temperatures to rise, thus lowering the fracture strength of the AA7075 alloy, and even to reach its incipient melting temperature (480–485 °C), as a small volume fraction of residual phases with a low melting point remained in the alloy. It is now clear that at the same extrusion speed, the surface appearance is not sensitive enough to distinguish the three extrusion die designs in terms of the extrudate surface quality. In other words, extrusion speed has a stronger effect on the surface quality of the extrudate through its effect on the extrudate temperature.

4.3. *Extrusion pressure*

FEM simulation was also utilized to indicate the effects of die bearing length setting and ram speed on extrusion pressure. From Fig. 14 it can be seen that the effect of die bearing length on extrusion pressure is rather marginal. Die No. 3 leads to the highest breakthrough pressure, because of the longest bearing lengths, the largest contact areas at the die bearing and the lowest workpiece temperatures as shown earlier.

The effect of ram speed on extrusion pressure is shown in Fig. 15. The difference in extrusion pressure appears to be also insignificant. The pressure curve of the extrusion cycle at a ram speed of 0.4 mm/s is at a slightly lower level in comparison with that at 0.6 mm/s. Obviously, this is caused by higher flow stresses at higher strain rates (Prassad and Sasidhara, 1997). It is known that the flow stress of the AA7075 alloy is more sensitive to strain rate than softer aluminium alloys (Lee et al., 2000). However, in achieving a high extrusion throughput, extrusion pressure appears to be a far less important limiting factor in comparison with extrudate temperature.

5. Conclusions

In the present case study, the effects of die bearing length and ram speed on extrudate temperature and extrusion pressure were predicted by means of 3D FEM simulation and validated by extrusion experiments. This has been found that in the case of extruding the 7075 aluminium alloy, the extrudate temperature is affected by die design, but more strongly by ram speed. A larger bearing length allows more heat to dissipate to the colder die when there are temperature differences between the die and workpiece, thus giving a wider scope for extrusion process optimization. The extruded profile has more stable dimensions after exiting from the die with a longer bearing. The effects of die design and ram speed on extrusion pressure are both marginal. Extrusion speed has a strong effect on extrudate temperature and the latter, rather than extrusion pressure, is the primary limiting factor for a high extrusion throughput.

REFERENCES

Arentoft, M., Gronostajski, Z., Niechajowicz, A., Wanheim, T., 2000. Physical and mathematical modelling of extrusion processes. J. Mater. Process. Technol. 106, 2–7.

Dixon, B., Extrusion of 2xxx and 7xxx alloys 2000. Proceedings of the 7th International Aluminium Extrusion Technology Seminar, vol. 1. Aluminium Association and Aluminium Extruder's Council, Wauconda, Illinois, pp. 281–294.

Flitta, I., Sheppard, T., 2003. Nature of friction in extrusion process and its effect on material flow. Mater. Sci. Technol. 19, 837–846.

Gouveia, B.P.P.A., Rodrigues, J.M.C., Martins, P.A.F., Bay, N., 2001. Physical modelling and numerical simulation of the round-to-square forward extrusion. J. Mater. Process. Technol. 112, 244–251.

Johnson, W., Kudo, H., 1962. The Mechanics of Metal Extrusion. Manchester University Press, Manchester, p. 60.

Kayser, T., Parvizian, F., Hortig, C., Svendsen, B., 2008. Advances on extrusion technology and simulation of light alloys. Key Eng. Mater. 367, 117–123.

Lee, W.-S., Sue, W.-C., Lin, C.-F., Wu, C.-J., 2000. The strain rate and temperature dependences of the dynamic impact properties of 7075 aluminium alloy. J. Mater. Process. Technol. 100, 116–122.

Lee, G.-A., Kwak, D.-Y., Kim, S.-Y., Im, Y.-T., 2002. Analysis and design of flat-die hot extrusion process 1. Three-dimensional finite element analysis. Int. J. Mech. Sci. 44, 915–934.

Li, Q., Smith, C.J., Harris, C., Jolly, M.R., 2003a. Finite element investigations upon the influence of pocket die designs on metal flow in aluminium extrusion, part I, effect of pocket angle and volume on metal flow. J. Mater. Process. Technol. 135, 189–196.

Li, L., Zhou, J., Duszczyk, J., 2003b. Prediction of temperature evolution during the extrusion of 7075 aluminium alloy at various ram speeds. J. Mater. Process. Technol. 145, 360–370.

Prassad, Y.V.R.K., Sasidhara, S., 1997. Hot Working Guide: A Compendium of Processing Maps. ASM International, Materials Park, Ohio, pp. 139–141.

Sheppard, T., Tunnicliffe, P.J., Patterson, S.J., 1982. Direct and indirect extrusion of a high strength aerospace alloy (AA7075). J. Mech. Work. Technol. 6, 313–331.

Shikorra, M., Donati, L., Tomesani, L., Tekkaya, A.E., 2007. Extrusion Benchmark 2007—benchmark experiments: study on material flow extrusion of a flat die. Key Eng. Mater. 367, 1–8.

Zakharov, V.V., 2005. Scientific aspects of deformability of aluminium alloys during extrusion. Adv. Perform. Mater. 2, 51–66.

Zhou, J., Li, L., Duszczyk, J., 2003. 3D FEM simulation of the whole cycle of aluminium extrusion throughout the transient state and the steady state using the updated Lagrangian approach. J. Mater. Process. Technol. 134, 383–397.